Preprints.org

Article

Not peer-reviewed version

Deep Learning–Based Automated Segmentation and Quantification of Ellipsoid Zone and RPE–Bruch's Membrane Complex in Healthy Subjects and Geographic Atrophy

Nasiq Hasan [†] , Adarsh Gadari [†] , Sharat Chandra Vupparaboina , Elham Sadeghi , Giulia Gregori , Utkarsh Doshi , José-Alain Sahel , Sandeep Chandra Bollepalli , Kiran Kumar Vupparaboina , Jay Chhablani [*]

Posted Date: 21 April 2026

doi: 10.20944/preprints202604.1517.v1

Keywords: deep learning; artificial intelligence; ellipsoid zone; RPE-Bruch's membrane

Preprints.org is a free multidisciplinary platform providing preprint service that is dedicated to making early versions of research outputs permanently available and citable. Preprints posted at Preprints.org appear in Web of Science, Crossref, Google Scholar, Scilit, Europe PMC.

Copyright: This open access article is published under a Creative Commons CC BY 4.0 license, which permit the free download, distribution, and reuse, provided that the author and preprint are cited in any reuse.

Preprints.org (www.preprints.org) | NOT PEER-REVIEWED | Posted: 21 April 2026 doi:10.20944/preprints202604.1517.v1

Disclaimer/Publisher's Note: The statements, opinions, and data contained in all publications are solely those of the individual author(s) and contributor(s) and not of MDPI and/or the editor(s). MDPI and/or the editor(s) disclaim responsibility for any injury to people or property resulting from any ideas, methods, instructions, or products referred to in the content.

Article

Deep Learning–Based Automated Segmentation and Quantification of Ellipsoid Zone and RPE–Bruch's Membrane Complex in Healthy Subjects and Geographic Atrophy

Nasiq Hasan [1,†], Adarsh Gadari [2,†], Sharat Chandra Vupparaboina [2], Elham Sadeghi [1], Giulia Gregori [1,3], Utkarsh Doshi [2], José-Alain Sahel [1,2], Sandeep Chandra Bollepalli [2], Kiran Kumar Vupparaboina [2] and Jay Chhablani [1,2,*]

[1] University of Pittsburgh Medical Center, Pittsburgh, PA, USA
[2] University of Pittsburgh, Pittsburgh, PA, USA
[3] Eye Clinic, Department of Experimental and Clinical Medicine, Polytechnic University of Marche, Ancona, Italy
* Correspondence: jay.chhablani@gmail.com
† These authors contributed equally to this work.

Abstract

Purpose: To validate a deep learning algorithm for automated segmentation and quantitative assessment of the ellipsoid zone (EZ) and RPE–Bruch's membrane (BM) complex in healthy and geographic atrophy (GA) eyes. **Methods:** In this retrospective study, SD-OCT volume scans from 30 healthy and 30 eyes with GA were analysed. NMI-Outer Retina Analyzer was used to segment the inner EZ, inner RPE, and outer BM. Average thicknesses of EZ-RPE, EZ-BM, and RPE-BM were calculated from volumes and across nine ETDRS sectors. Manual segmentations were corrected by two masked expert graders and were compared using ICC. Dice coefficients (DC), Pearson correlation, and absolute thickness differences were used to assess agreement between automated and manual segmentation. Heat maps were generated to visualize thicknesses. **Results:** Thirty healthy eyes and thirty GA eyes were included in the analysis. Mean EZ–RPE, EZ–BM, and RPE–BM thicknesses were 47.55 ± 6.75 μm, 69.49 ± 6.92 μm, and 21.94 ± 3.46 μm, in the healthy eyes and 15.65 ± 11.09 μm, 39.18 ± 23.28 μm, and 23.52 ± 16.21 μm in GA eyes respectively. The model demonstrated high segmentation accuracy, with mean DC of 0.998 in healthy eyes and 0.995–0.998 in GA eyes. In healthy eyes, differences between automated and manual measurements were minimal (1.42 ± 3.39 μm (2.98%) for EZ–RPE, 1.31 ± 3.18 μm (1.88%) for EZ–BM, and 0.67 ± 1.71 μm (3.05%) for RPE–BM) which is within 1.88-3.05% from the gold standard (manual corrections), whereas GA eyes showed greater variability (mean differences of 3.61 ± 8.62 μm (23.06%) for EZ–RPE, 4.28 ± 11.34 μm (10.92%) for EZ–BM, and 4.4 ± 10.45 μm (18.71%) for RPE–BM). Heat maps revealed increased variability at the junctional zone surrounding atrophy. Automated and manual measurements showed strong correlations across all sectors in GA eyes (r = 0.97 for EZ–BM, 0.96 for EZ–RPE, and 0.89 for RPE–BM). **Conclusions:** The NMI-ORA enables accurate, automated segmentation and quantification of outer retinal layers, with performance comparable to expert graders.

Keywords: deep learning; artificial intelligence; ellipsoid zone; RPE-Bruch's membrane

© 2026 by the author(s). Distributed under a Creative Commons CC BY license.

Preprints.org (www.preprints.org) | NOT PEER-REVIEWED | Posted: 21 April 2026 doi:10.20944/preprints202604.1517.v1

1. Introduction

Age-related macular degeneration (AMD) is the leading cause of vision loss in the elderly, affecting approximately 200 million people worldwide, with prevalence projected to reach 288 million by 2040. Geographic atrophy (GA) represents an advanced stage of AMD and is associated with irreversible vision loss[1,2]. Recently, two intravitreal agents, (Syfovre; Apellis Pharmaceuticals, Waltham, MA, USA) or avacincaptad pegol (Izervay; Iveric Bio, Inc., Parsippany, NJ, USA)., have received food and drug administration (FDA) approval for GA, targeting disease progression in patients with established atrophy and baseline visual decline[3]. Pivotal trials supporting these approvals relied on fundus autofluorescence (AF) to quantify GA, defining lesions as hypoautofluorescent areas with a minimum size of 250 μm[4]. However, therapeutic options remain unavailable for earlier stages of AMD, when intervention might offer the greatest potential to prevent progression to GA and subsequent vision loss.

GA is characterized by complete loss of the outer retina and retinal pigment epithelium (RPE). However, degeneration of the outer retinal layers precedes RPE loss[5]. Increasing attention has also been directed toward the junctional zone, although its definition remains inconsistent. It is described in some studies as a 100 μm margin surrounding atrophy[6], and in others as areas with outer retinal loss in the presence of intact RPE[7]. These observations highlight the importance of the outer retinal bands, which may be equally, if not more, relevant than the RPE in understanding the pathophysiology and progression of AMD. Among these bands, the ellipsoid zone (EZ) has been most commonly evaluated, both qualitatively and quantitatively, as a biomarker of outer retinal integrity. The ellipsoid zone (EZ), previously referred to as the inner segment–outer segment (IS/OS) junction, represents the interface of photoreceptor inner and outer segments on optical coherence tomography (OCT). It is one of the four hyperreflective outer retinal bands located between the external limiting membrane (ELM) and the interdigitation zone. Photoreceptors are highly metabolically active cells with a dense concentration of mitochondria within the ellipsoid portion of the inner segment which correspond to the ellipsoid zone. Owing to the high reflectivity of these mitochondria, the EZ appears as a distinct hyperreflective band on OCT[8].

With the newer drugs in the pipeline, there has been a paradigm shift from AF to OCT and en face OCT as preferred modalities for quantifying photoreceptor and RPE loss in retinal diseases, including AMD[9]. Clinical trials in macular telangiectasia have already adopted EZ loss as a structural endpoint[10,11]. Compared with AF, OCT B-scans and en face imaging provide superior structural detail of the EZ and RPE. In GA, a comparative study demonstrated good correlation between AF and OCT based measurements of progression, although baseline RPE loss was overestimated on AF, likely due to contributions from RPE alterations and thinning to the hypoautofluorescent signal[12]. Another study reported that retinal sensitivity correlated strongly with photoreceptor damage rather than RPE damage, and RPE loss alone was not predictive of functional decline[13].

Accurate identification and segmentation of the outer retinal bands remain challenging, particularly in diseased eyes. Advances in imaging led to the development of automated segmentation models using traditional image processing and advanced deep learning methods. However, the performance of deep learning methods depends on the training data and the quality of manual annotations. Since, annotating the layers like EZ, RPE and Bruch's membrane is time consuming and induces fatigue to the annotator, leading to the degradation of annotations, utilization of advanced DL methods is often limited in practice. . In the light of these challenges, we validate a tool that enables near-accurate segmentation of the EZ and RPE–Bruch's membrane complex in both healthy and GA eyes, along with quantitative assessment of these layers, providing a potential for future clinical trials and clinical practice.

© 2026 by the author(s). Distributed under a Creative Commons CC BY license.

Preprints.org (www.preprints.org) | NOT PEER-REVIEWED | Posted: 21 April 2026 doi:10.20944/preprints202604.1517.v1

2. Methods

2.1. Dataset

This retrospective study was conducted in the Department of Ophthalmology at the University of Pittsburgh Medical Center, in accordance with the Declaration of Helsinki and approved by the Institutional Review Board. OCT volume scans from 30 healthy eyes of participants aged more than 55 years and 30 eyes with geographic atrophy were analyzed for automated segmentation of the EZ and RPE–Bruch's membrane complex. This retrospective study utilized archived OCT scans obtained from the institutional imaging database. Data were accessed for between 15 January 2025 and 30 March 2025. The investigators had access only to limited clinical information, including patient age and diagnosis. No direct identifiers (such as names, medical record numbers, or contact information) were available to the study team during or after data collection.

Spectral-domain OCT volume scans were obtained using the Heidelberg Spectralis system. Scans with a quality score <20 were excluded. For healthy eyes, a 49-raster protocol was used, while eyes with GA were imaged with a 97 raster protocol. All scans covered a 6 × 6 mm area centered on the fovea, with each B-scan consisting of 512 × 496 pixels. The Early Treatment Diabetic Retinopathy Study (ETDRS) grid was applied to delineate subfields, including the central 1-mm foveal zone, the 3-mm inner ring (superior, temporal, inferior, and nasal), and the 6-mm outer ring (superior, temporal, inferior, and nasal).

2.2. Algorithm

Proprietary software developed by the NetraMind Innovations (NMI) called NMI-ORA(Outer Retina Analyzer) was used to automatically segment three outer retinal layers, the inner border of the EZ, the inner border of the RPE, and the outer border of Bruch's membrane (BM). NMI-ORA. The proposed algorithm employs a two-module framework designed to achieve accurate and biologically consistent layer segmentation. The first module integrates deep learning techniques with pseudo-labeling strategies and traditional image processing methods to delineate retinal layers. The second module, a deep learning model for geographic atrophy (GA) segmentation, detects GA regions and aligns the EZ and RPE boundaries with the BM boundary in accordance with pathological features. Together, these modules operate synergistically to improve segmentation reliability. Algorithm performance was evaluated by quantifying the extent of manual correction required to address segmentation errors, based on the practical observation that adjusting existing boundaries demands considerably less effort than annotating them de novo. Evaluation metrics included mean difference, mean absolute difference, and correlation coefficient, computed for each segmented boundary across A-scan, B-scan, volumetric, and ETDRS-grid levels of analysis.

2.3. Evaluation

Following automated segmentation, two masked experienced graders (NH and GG) performed manual corrections of retinal layer boundaries where necessary. Three thickness parameters were defined: EZ-RPE thickness (inner ellipsoid zone to inner RPE), EZ-BM thickness (inner ellipsoid zone to outer Bruch's membrane), and RPE-BM thickness (inner RPE to outer Bruch's membrane). Inter-grader agreement was calculated, and any discrepancies were resolved by consulting the senior author (JC) for the final decision. The outer EZ boundary was excluded from calculations due to the frequently indistinct demarcation between the ellipsoid zone and interdigitation zone in pathological tissue, particularly in AMD cases with geographic atrophy. Thickness measurements were calculated for both automated and manually corrected segmentations to enable comparative analysis.

Average thickness measurements for the EZ-RPE, EZ-BM, and RPE-BM layers were computed across the entire scan volume and within the nine standardized ETDRS subfields. These calculations were performed on both the automated segmentations and manual corrections. The absolute differences between automated and manual thickness values were subsequently analyzed to quantify

© 2026 by the author(s). Distributed under a Creative Commons CC BY license.

Preprints.org (www.preprints.org) | NOT PEER-REVIEWED | Posted: 21 April 2026 doi:10.20944/preprints202604.1517.v1

segmentation accuracy. Additionally, pixel-wise discrepancies between automated and manual segmentation boundaries were assessed for all three retinal layers.

2.4. Statistical Analysis

Statistical analyses were performed using Python. Thickness values were expressed as mean ± standard deviation, calculated from individual A-scan measurements. Average volume thicknesses and nine ETDRS subfield thicknesses were measured for all three layers. Interobserver variability was assessed using the intraclass coefficient (ICC). The Dice coefficient (DC) was used to assess agreement between automated and manually corrected segmentations, and Pearson correlation was used to assess the relationship between automatically measured and manually corrected thickness values.

3. Results

A total of 60 eyes of 60 patients were included in the final analysis. In the healthy subgroup (30 eyes), the mean patient age was 63.11 ± 6.46 years, with 16/30 (53.3%) females. Mean thicknesses were 47.55 ± 6.75 μm for EZ–RPE, 69.49 ± 6.92 μm for EZ–BM, and 21.94 ± 3.46 μm for RPE–BM. In the GA subgroup (30 eyes), the mean age was 72.21 ± 10.41 years, with 21/30 (70%) females. The mean GA area was 8.57 mm^2, and the total EZ loss area was 13.29 mm^2. Mean thicknesses were 15.65 ± 11.09 μm (EZ–RPE), 39.18 ± 23.28 μm (EZ–BM), and 23.52 ± 16.21 μm (RPE–BM). (Table 1) Mean EZ–RPE volume was 1.71 ± 0.24 mm^3 in healthy eyes and 0.56 ± 0.38 mm^3 in eyes with GA.

Table 1. - Mean thicknesses following automated segmentation and manual correction, and absolute difference in thickness of the three layers in healthy and AMD subjects.

Group	Layer	Manual correction (microns)	Automated measurement (microns)	Thickness difference (microns)
Healthy	EZ-BM	69.49+/-6.92	69.74+/-5.84	1.31+/-3.18
	EZ-RPE	47.55+/-6.75	47.72+/-5.68	1.42+/-3.39
	RPE -BM	21.94+/-3.46	22.02+/-3.57	0.67+/-1.71
AMD	EZ-BM	39.18+/-23.28	38.67+/-23.64	4.28+/-11.34
	EZ-RPE	15.65+/-11.09	17.09+/-13.06	3.61+/-8.62
	RPE -BM	23.52+/-16.21	21.66+/-14.91	4.4+/-10.45

EZ- Ellipsoid zone, RPE - Retinal pigment epithelium, BM – Bruchs membrane.

The segmentation approach performed comparably to a retina expert, with only a small number of scans requiring manual corrections at select points on the B-scan (Fig 1). The ICC between two manual graders was 0.97 (95% CI -0.94-0.99). In healthy eyes, the average difference between manual and automated layer thicknesses was 1.42 ± 3.39 μm (2.98%) for EZ–RPE, 1.31 ± 3.18 μm (1.88%) for EZ–BM, and 0.67 ± 1.71 μm (3.05%) for RPE–BM, which is within 1.88-3.05% from the gold standard (manual corrections). Among GA eyes, variability between manual and automated measurements was higher, with mean differences of 3.61 ± 8.62 μm (23.06%) for EZ–RPE, 4.28 ± 11.34 μm (10.92%) for EZ–BM, and 4.4 ± 10.45 μm (18.71%) for RPE–BM. On examining the heat maps of the difference in absolute thicknesses, we observed that the junctional area around the atrophy contributed to higher differences between the two measurements. (Fig 2)

In the healthy group, the mean DC comparing manual and automated segmentation was 0.998 for all three boundaries. In the GA subgroup, the coefficients ranged from 0.995 to 0.996. Absolute differences in pixels and DC between manual and automated segmentation are summarized in Table 2. When evaluating variability across different ETDRS grid sectors, the average absolute thickness differences ranged from 0.58–1.31 μm for EZ–BM, 0.78–1.39 μm for EZ–RPE, and 0.49–0.91 μm for

© 2026 by the author(s). Distributed under a Creative Commons CC BY license.

Preprints.org (www.preprints.org) | NOT PEER-REVIEWED | Posted: 21 April 2026 doi:10.20944/preprints202604.1517.v1

RPE–BM, with higher variability observed in the inner nasal and all outer sectors (Table 3). The mean DC of the boundaries were 0.998 in healthy eyes and ranged from 0.995 to 0.998 in GA eyes (Table 4). Pearson correlation demonstrated good agreement between automatically measured and manually measured thickness values within all sectors, with coefficients of 0.97 for EZ–BM, 0.96 for EZ–RPE, and 0.89 for RPE–BM among the GA eyes (Fig 3).

Table 2. - Mean absolute difference in pixels and Dice coefficient of the three layers in healthy and AMD subjects.

Group	Boundary	Absolute difference (pixels)	Dice coefficeint
Healthy	EZ	0.249+/-0.757	0.998+/-0.007
	RPE	0.172+/-0.454	0.998+/-0.006
	BM	0.142+/-0.365	0.998+/-0.001
AMD	EZ	1.25+/-3.83	0.995+/-0.013
	RPE	1.33+/-3.85	0.995+/-0.014
	BM	0.71+/-2.74	0.996+/-0.013

EZ- Ellipsoid zone, RPE - Retinal pigment epithelium, BM – Bruchs membrane, AMD – Age related macular degeneration.

Table 3. - Mean manual, automated thicknesses and absolute difference in thickness within the nine sectors in healthy subjects.

Layer	EZ-BM			EZ-RPE			RPE-BM		
Sector	Manual measurement	Automated measurement	Absolute difference	Manual measurement	Automated measurement	Absolute difference	Manual measurement	Automated measurement	Absolute difference
Foveal	77.34+/-5.21	77.26+/-4.94	0.69+/-1.59	52.94+/-5.88	52.73+/-5.46	0.85+/-1.90	24.40+/-2.81	24.53+/-2.82	0.56+/-1.35
Inner inferior	72.73+/-4.53	72.58+/-4.31	0.79+/-1.75	49.34+/-4.81	49.07+/-4.62	0.94+/-2.02	23.39+/-2.99	23.51+/-3.16	0.59+/-1.42
Inner nasal	73.71+/-4.61	73.26+/-4.42	1.04+/-1.86	50.28+/-4.86	49.70+/-4.71	1.20+/-2.11	23.43+/-2.81	23.57+/-3.03	0.67+/-1.53
Inner superior	72.50+/-3.73	72.42+/-3.62	0.58+/-1.43	49.11+/-4.26	48.84+/-4.31	0.78+/-1.77	23.39+/-2.89	23.58+/-3.10	0.60+/-1.48
Inner temporal	72.46+/-4.69	72.46+/-4.51	0.69+/-1.59	47.96+/-5.28	47.77+/-4.95	0.92+/-2.00	24.50+/-3.36	24.69+/-3.45	0.78+/-1.70
Outer inferior	69.47+/-5.39	69.65+/-4.62	1.31+/-2.78	48.24+/-5.37	48.43+/-4.56	1.35+/-2.85	21.23+/-2.36	21.22+/-2.33	0.49+/-1.26
Outer nasal	69.39+/-5.31	69.23+/-4.85	1.29+/-2.36	47.96+/-5.26	47.72+/-4.86	1.39+/-2.57	21.43+/-2.45	21.51+/-2.68	0.61+/-1.51
Outer superior	69.40+/-4.80	69.65+/-4.01	0.94+/-2.27	47.88+/-5.06	48.07+/-4.34	1.02+/-2.34	21.53+/-2.48	21.59+/-2.56	0.52+/-1.31
Outer temporal	69.62+/-5.13	69.76+/-4.87	1.06+/-2.21	47.14+/-5.20	47.12+/-4.75	1.24+/-2.59	22.48+/-3.04	22.64+/-3.19	0.91+/-1.91

EZ- Ellipsoid zone, RPE - Retinal pigment epithelium, BM – Bruchs membrane.

© 2026 by the author(s). Distributed under a Creative Commons CC BY license.

Preprints.org (www.preprints.org) | NOT PEER-REVIEWED | Posted: 21 April 2026 doi:10.20944/preprints202604.1517.v1

Table 4. - Dice coefficients of the three boundaries within the nine sectors in healthy and AMD patients.

ETDRS sector	Healthy			AMD		
	EZ	RPE	BM	EZ	RPE	BM
Foveal	0.999+/-0.001	0.999+/-0.001	0.999+/-0.001	0.996+/-0.008	0.996+/-0.007	0.996+/-0.002
Inner inferior	0.999+/-0.001	0.999+/-0.001	0.999+/-0.001	0.997+/-0.008	0.996+/-0.007	0.998+/-0.002
Inner nasal	0.999+/-0.001	0.999+/-0.001	0.999+/-0.001	0.997+/-0.011	0.997+/-0.009	0.998+/-0.004
Inner superior	0.999+/-0.001	0.999+/-0.001	0.999+/-0.001	0.996+/-0.007	0.996+/-0.007	0.997+/-0.004
Inner temporal	0.999+/-0.001	0.999+/-0.001	0.999+/-0.001	0.995+/-0.007	0.995+/-0.006	0.997+/-0.002
Outer inferior	0.999+/-0.001	0.999+/-0.001	0.999+/-0.001	0.997+/-0.008	0.997+/-0.007	0.998+/-0.003
Outer nasal	0.999+/-0.001	0.999+/-0.001	0.999+/-0.001	0.997+/-0.011	0.997+/-0.008	0.998+/-0.005
Outer superior	0.999+/-0.001	0.999+/-0.001	0.999+/-0.001	0.996+/-0.008	0.995+/-0.008	0.997+/-0.005
Outer temporal	0.999+/-0.001	0.999+/-0.001	0.999+/-0.001	0.996+/-0.009	0.997+/-0.008	0.998+/-0.003

EZ- Ellipsoid zone, RPE - Retinal pigment epithelium, BM – Bruchs membrane.

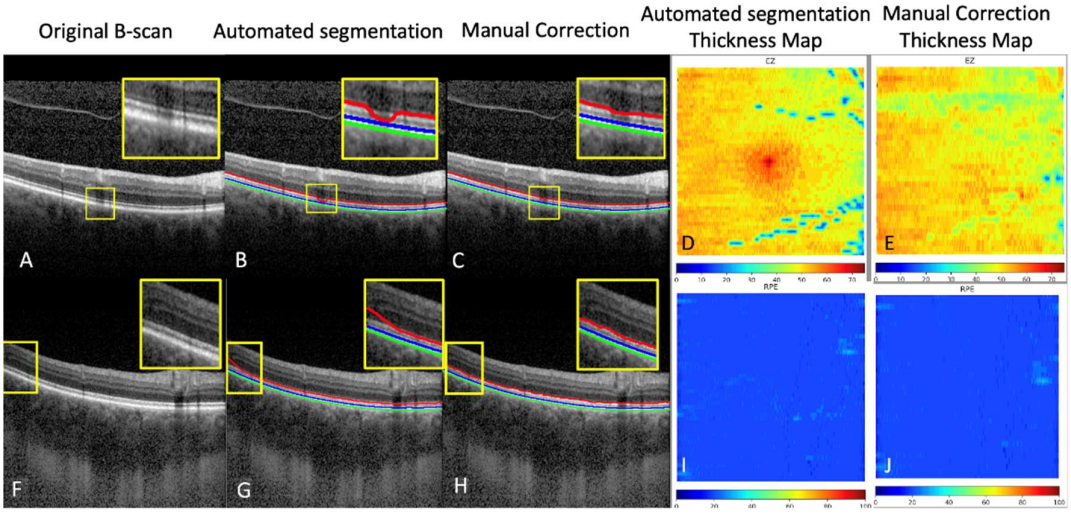

Figure 1. Representative B-scans showing original (A,F) automated segmentation (B,G) and manual corrections (C,H). Yellow boxes indicate areas of segmentation error, beneath retinal vessel shadowing (B) and at scan edges (G). Corresponding EZ–RPE (D, E) and RPE–BM (I,J) thickness heatmaps are displayed before and after manual correction. Automated maps demonstrate that most segmentation errors in EZ–RPE thickness occur along the vascular arcades (D).

© 2026 by the author(s). Distributed under a Creative Commons CC BY license.

Preprints.org (www.preprints.org) | NOT PEER-REVIEWED | Posted: 21 April 2026 doi:10.20944/preprints202604.1517.v1

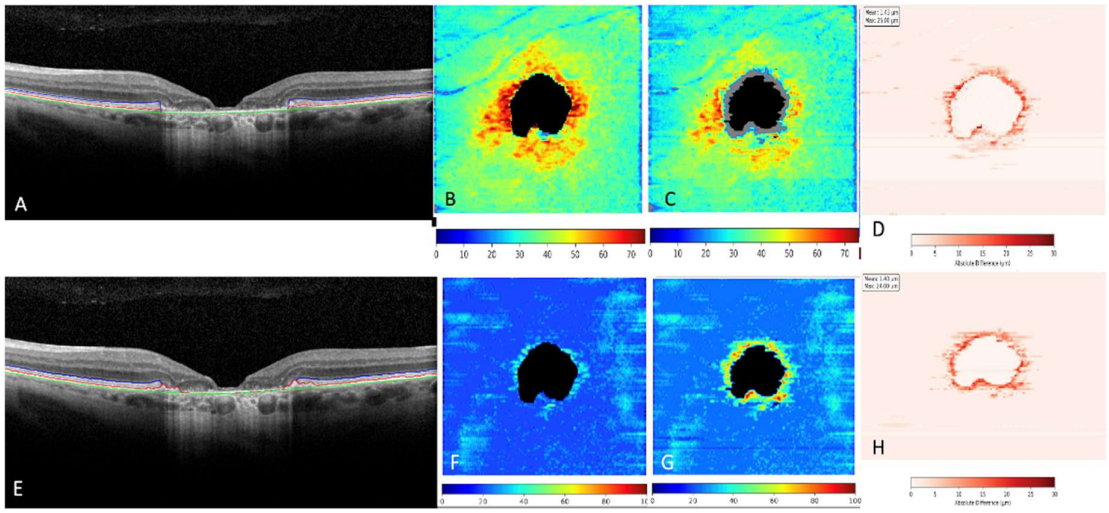

Figure 2. Foveal B-scan demonstrating automated (A) versus manually corrected segmentation € of the outer retinal layers. Corresponding EZ–RPE (B,C) and RPE–BM thickness (F,G) heatmaps are shown for both automated and manually corrected segmentation. The manually corrected EZ–RPE map highlights the area of EZ loss (gray) surrounding the geographic atrophy. The rightmost heatmap displays the absolute differences (D,H) between automated and manual segmentation, with the greatest corrections observed at the junctional zone around the geographic atrophy.

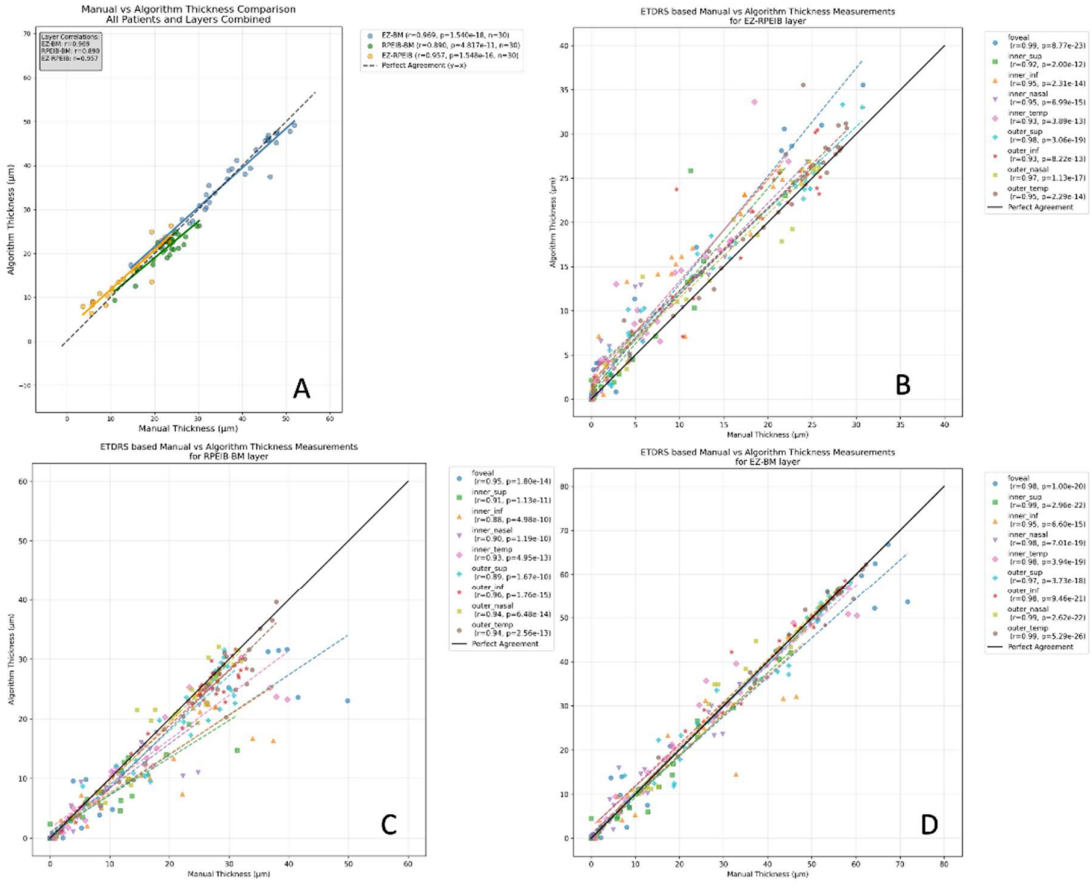

Figure 3. Scatter plots comparing automated versus manual corrections derived thickness of EZ-RPE, RPE-BM and EZ-BM among AMD patients (A). The dashed lines show the best-fit regression lines for each thickness, with corresponding Pearson correlation coefficients (r) and p-values shown in the legend. B,C and D shows scatter plots comparing automated versus manual corrections derived sectoral thickness measurements of EZ-

© 2026 by the author(s). Distributed under a Creative Commons CC BY license.

Preprints.org (www.preprints.org) | NOT PEER-REVIEWED | Posted: 21 April 2026 doi:10.20944/preprints202604.1517.v1

RPE, RPE-BM and EZ-BM respectively. The algorithm demonstrates strong correlation with manual measurements across all regions, with the highest agreement observed within the fovea.

4. Discussion

Our study demonstrates a deep learning–based, high-performance automated model for segmentation of the EZ and RPE–BM in both healthy eyes and eyes with AMD related GA. The results indicate that automated segmentation and thickness measurements closely approximate manual annotations by experienced retinal graders with Dice coefficients of 0.998 in healthy subjects and 0.995-0.998 among GA eyes

Advances in OCT resolution have allowed the outer retinal layers to be delineated into four distinct bands, and high-resolution OCT imaging has revealed additional sublayers with remarkable clarity[14]. Despite this, visualizing all layers in routine clinical practice and translating these observations into applications for retinal disease remains challenging. Nonetheless, the four primary outer retinal bands remain the standard reference, with the more hyperreflective layers, particularly the RPE–Bruch's complex and the ellipsoid zone, commonly used for both qualitative and quantitative assessment across various retinal pathologies.

Miranda et al. were among the few to report Dice coefficients for individual retinal layer segmentation, including the ellipsoid zone (EZ). They validated the BioImagingLab/INESC TEC deep learning model against the gold standard of manually corrected automatic segmentation from the Heidelberg Spectralis HRA+OCT software (Version 6.16.8.0)[15]. Dice scores were excellent for most retinal layers in healthy controls (0.928–0.995), particularly the inner retina, but were lower for EZ segmentation (0.783). A similar reduction in EZ accuracy was observed in both intermediate and exudative AMD, despite high performance for other retinal layers and for fluid in exudative AMD. Another group evaluated DL-based retinal layer segmentation of the inner limiting membrane, RPE inner boundary, and Bruch's membrane using U-Net and DeepLabV3. Their models, trained on Spectralis SD-OCT data and tested on both Spectralis and Cirrus devices, achieved Dice scores of 0.76–0.87, though they did not assess EZ[16]. For patients without AMD, Dice coefficients ranged from 0.83 to 0.84. A study on using the same algorithm in patients with hydroxychloroquine toxicity showed a DICE coefficient of 0.74+/- 0.23[17]. In comparison, our model achieved superior performance in retinal layer segmentation, including the EZ.

Most DL studies have focused on segmenting EZ and RPE loss and attenuation, showing high accuracy in detecting regions of GA and EZ disruption. This approach mainly emphasizes spatial overlap of EZ and RPE loss areas rather than assessing the precision of thickness quantification, leaving a gap in literature regarding the validation of thickness measurements using Dice metrics. Using absolute EZ thickness may enhance clinical trials by providing quantitative measures rather than classifying regions simply as partial or complete attenuation. Such measurements allow evaluation of different levels of EZ risk, and future studies could define thickness thresholds around the GA penumbra associated with mild, moderate, or high risk.

Recent studies have utilized ellipsoid zone morphology to monitor geographic atrophy progression and to evaluate the efficacy of drugs aimed at slowing or halting disease progression. These metrics have been incorporated as clinical trial endpoints in recent studies, including ReCLAIM-2[18] and FILLY[19]. Orlando et al. reported a Dice coefficient of 0.912 ± 0.021 for the central subfield and 0.907 ± 0.028 for the full sample when comparing automated segmentation to manual grading of photoreceptor layer (EZ-RPE) in diabetic retinopathy eyes[20]. Wang et al. evaluated an EZ loss detection algorithm based on thresholding of thickness maps derived from layer segmentation, reporting Dice coefficients of 0.88 ± 0.07 for B scan based segmentation and 0.63 ± 0.25 for EZ loss detection, as assessed against manual grading of B-scans and ratio images[21]. Similarly, a study by Zhang et al established a model that automatically classified atrophy as cRORA or iRORA based on RPE loss, photoreceptor degeneration, and hypertransmission, demonstrating excellent performance that exceeded human-to-human consensus[22]. A recent study by Kalra et al. also reported excellent accuracy, with 99% detection of EZ at risk and 90% measurement accuracy[23].

© 2026 by the author(s). Distributed under a Creative Commons CC BY license.

Preprints.org (www.preprints.org) | NOT PEER-REVIEWED | Posted: 21 April 2026 doi:10.20944/preprints202604.1517.v1

However, the analysis of these studies focused on the area of atrophy or EZ at risk rather than direct thickness measurements of the retinal layers.

Automated and manual segmentation showed greater variability in GA patients compared to healthy controls, particularly within the junctional zone, where differences of upto 25 μm were observed on heat maps. This variability may reflect deposits or abrupt changes in outer retinal morphology. Since the junctional zone is a key area of interest in GA trials, its analysis of the EZ and other outer retinal layers is especially important. Although the absolute variability was small, the relative percentage shift appeared significant. Minimal manual correction at these points could improve accuracy. We did not assess average thickness across different AMD sectors due to heterogeneity in GA location within our cohort. Future studies should examine junctional zone thickness in greater detail, ideally at set distances (e.g., 100, 200, and 300 μm from the GA margin) and compare these with normal EZ thickness in the scan periphery.

One of the key advantages of our tool is that it enables manual correction, allowing human graders to verify the accuracy of automated segmentation and perform manual corrections when needed. Moreover, the time required for manual correction is substantially reduced, from several hours to less than 15 minutes even in poor-quality OCT volumes. Our model also enables the generation of maps that allow independent measurement of EZ and RPE attenuation and loss and can be further stratified into different levels of risk, which can serve as biomarkers in major clinical trials. The associated heat maps provide a qualitative assessment of GA progression, offering an alternative to reliance on fundus autofluorescence. By comparing EZ and RPE heat maps, areas of the retina at risk can be identified both qualitatively and quantitatively, facilitating evaluation of current and emerging interventions for AMD and GA. This algorithm is readily applicable in both clinical trial settings and routine clinical practice.

Limitations of this study include training and validation of the model using a single OCT device, albeit one that is widely available and commonly used in clinical trials. The sample size was considerably small, however, the algorithm was trained and tested with an external validation dataset. Manual evaluation of OCT scans at this level requires expert graders and is inherently labor-intensive, with potential for intergrader variability and measurement bias. These limitations hinder the feasibility of using such assessments in routine clinical practice or as efficacy endpoints in clinical studies. A fully automated three-dimensional quantitative grading system, however, can substantially reduce the time required to analyze each volume.

5. Conclusions

We present a novel, fully automated deep-learning method for the detection, quantification, and classification of geographic atrophy from OCT scans. The model demonstrated predictive performance comparable to that of clinical experts. This approach has the potential to support patient management and to standardize clinical trial endpoints, thereby facilitating the development of new therapies for GA.

Author Contributions: Conceptualization, NH, KKV and JC.; Methodology, NH, AG, KKV.; Software, AG, SCB and UD. Validation NH, GG, and ES.; Formal Analysis, NH and AG Investigation, NH and AG.; Resources, JC, JAS, KKV and SCB.; Data Curation, NH, GG and AG.; Writing NH and AG, X.X.; Writing – Review & Editing, JC and KKV. Visualization, KKV and JC Supervision, JC, KKV and SCB.; Project Administration, JC, JAS and KKV.; Funding Acquisition, JC, JAS and KKV.

Funding: Supported by NIH CORE Grant P30 EY08098 to the Department of Ophthalmology, the Eye and Ear Foundation of Pittsburgh, and an unrestricted grant from Research to Prevent Blindness, New York, NY and Shear Family Foundation.

Institutional Review Board: This retrospective study was conducted in accordance with the Declaration of Helsinki approved by the Institutional Review Board of University of Pittsburgh (STUDY20030263, April 3 2020).

Informed Consent Statement: Patient's consent was waived due to secondary research on data.

© 2026 by the author(s). Distributed under a Creative Commons CC BY license.

Preprints.org (www.preprints.org) | NOT PEER-REVIEWED | Posted: 21 April 2026 doi:10.20944/preprints202604.1517.v1

Data Availability Statement: The data that support the findings of this study are available from the corresponding author upon reasonable request. Due to patient privacy and institutional regulations, the data are not publicly available.

Disclosures: Nasiq Hasan, None; Adarsh Gadari, None; Sharat Chandra Vupparaboina, None; Elham Sadeghi, None; Giulia Gregori, None; Utkarsh Doshi, None; Jose-Alain **Sahel**, NetraMind Innovations (I), Pixium Vision (I), GenSight Biologics (I), Sparing Vision (I), Prophesee (I), Chronolife (I); , Sandeep Chandra **Bollepalli**, NetraMind Innovations (I); , Kiran Kumar **Vupparaboina**, NetraMind Innovations (I); , Jay **Chhablani**, NetraMind Innovations (O); Allergan (C), Novartis (C), Salutaris (C), OD-OS (C), Erasca (C), B&L (C), Iveric Bio (C), Ocular Therapeutics (I), AcuViz (I), Abbvie (I), Springer (R), Elsevier (R).

References

1. Pennington, K. L.; DeAngelis, M. M. Epidemiology of Age-Related Macular Degeneration (AMD): Associations with Cardiovascular Disease Phenotypes and Lipid Factors. *Eye Vis.* **2016**, *3*, 34.
2. Rein, D. B.; Wittenborn, J. S.; Zhang, X.; Honeycutt, A. A.; Lesesne, S. B.; Saaddine, J.; Vision Health Cost-Effectiveness Study Group. Forecasting Age-Related Macular Degeneration Through the Year 2050: The Potential Impact of New Treatments. *Arch. Ophthalmol.* **2009**, *127* (4), 533–540.
3. Csaky, K. G.; Miller, J. M. L.; Martin, D. F.; Johnson, M. W. Drug Approval for the Treatment of Geographic Atrophy: How We Got Here and Where We Need to Go. *Am. J. Ophthalmol.* **2024**, *263*, 231–239.
4. Holz, F. G.; Sadda, S. R.; Staurenghi, G.; Lindner, M.; Bird, A. C.; Blodi, B. A.; Bottoni, F.; Chakravarthy, U.; Chew, E. Y.; Csaky, K.; Curcio, C. A.; Danis, R.; Fleckenstein, M.; Freund, K. B.; Grunwald, J.; Guymer, R.; Hoyng, C. B.; Jaffe, G. J.; Liakopoulos, S.; Monés, J. M.; Oishi, A.; Pauleikhoff, D.; Rosenfeld, P. J.; Sarraf, D.; Spaide, R. F.; Tadayoni, R.; Tufail, A.; Wolf, S.; Schmitz-Valckenberg, S.; CAM group. Imaging Protocols in Clinical Studies in Advanced Age-Related Macular Degeneration: Recommendations from Classification of Atrophy Consensus Meetings. *Ophthalmology* **2017**, *124* (4), 464–478.
5. Mai, J.; Reiter, G. S.; Riedl, S.; Vogl, W.-D.; Sadeghipour, A.; Foos, E.; McKeown, A.; Bogunovic, H.; Schmidt-Erfurth, U. Quantitative Comparison of Automated OCT and Conventional FAF-Based Geographic Atrophy Measurements in the Phase 3 OAKS/DERBY Trials. *Sci. Rep.* **2024**, *14* (1), 20531.
6. Curcio, C. A.; Messinger, J.; Berlin, A.; Edwards, M. M.; McLeod, D. S.; Bijon, J.; Freund, K. B. Histology of Fundus Autofluorescence (FAF) in Multifocal Geographic Atrophy (GA) with Thick Choroid in Age-Related Macular Degeneration (AMD). *Invest. Ophthalmol. Vis. Sci.* **2024**, *65* (7), 2284.
7. Bearelly, S.; Chau, F. Y.; Koreishi, A.; Stinnett, S. S.; Izatt, J. A.; Toth, C. A. Spectral Domain Optical Coherence Tomography Imaging of Geographic Atrophy Margins. *Ophthalmology* **2009**, *116* (9), 1762–1769.
8. Litts, K. M.; Zhang, Y.; Freund, K. B.; Curcio, C. A. OPTICAL COHERENCE TOMOGRAPHY AND HISTOLOGY OF AGE-RELATED MACULAR DEGENERATION SUPPORT MITOCHONDRIA AS REFLECTIVITY SOURCES. *Retina Phila. Pa* **2018**, *38* (3), 445–461.
9. Schmidt-Erfurth, U.; Mai, J.; Reiter, G. S.; Riedl, S.; Vogl, W.-D.; Sadeghipour, A.; McKeown, A.; Foos, E.; Scheibler, L.; Bogunovic, H. Disease Activity and Therapeutic Response to Pegcetacoplan for Geographic Atrophy Identified by Deep Learning-Based Analysis of OCT. *Ophthalmology* **2025**, *132* (2), 181–193.
10. Pauleikhoff, D.; Pauleikhoff, L.; Chew, E. Y. Imaging Endpoints for Clinical Trials in MacTel Type 2. *Eye* **2022**, *36* (2), 284–293. https://doi.org/10.1038/s41433-021-01723-7.
11. Chew, E. Y.; Gillies, M.; Jaffe, G. J.; Gaudric, A.; Egan, C.; Constable, I.; Clemons, T.; Aaberg, T.; Manning, D. C.; Hohman, T. C.; Bird, A.; Friedlander, M.; MacTel CNTF NTMT-03 Research investigators. Cell-Based Ciliary Neurotrophic Factor Therapy for Macular Telangiectasia Type 2. *NEJM Evid.* **2025**, *4* (8),
12. Ehlers, J. P.; McConville, C.; Yordi, S.; Cetin, H.; Cakir, Y.; Kalra, G.; Amine, R.; Whitney, J.; Whitmore, V.; Bonnay, M.; Reese, J.; Clark, J.; Zhu, L.; Luo, D.; Jaffe, G. J.; Srivastava, S. K. Correlation Between Blue Fundus Autofluorescence and SD-OCT Measurements of Geographic Atrophy in Dry Age-Related Macular Degeneration. *Am. J. Ophthalmol.* **2024**, *266*, 92–101.
13. Takahashi, A.; Ooto, S.; Yamashiro, K.; Oishi, A.; Tamura, H.; Nakanishi, H.; Ueda-Arakawa, N.; Tsujikawa, A.; Yoshimura, N. Photoreceptor Damage and Reduction of Retinal Sensitivity Surrounding Geographic Atrophy in Age-Related Macular Degeneration. *Am. J. Ophthalmol.* **2016**, *168*, 260–268.

© 2026 by the author(s). Distributed under a Creative Commons CC BY license.

Preprints.org (www.preprints.org) | NOT PEER-REVIEWED | Posted: 21 April 2026 doi:10.20944/preprints202604.1517.v1

14. Chen, S.; Abu-Qamar, O.; Kar, D.; Messinger, J. D.; Hwang, Y.; Moult, E. M.; Lin, J.; Baumal, C. R.; Witkin, A.; Liang, M. C.; Waheed, N. K.; Curcio, C. A.; Fujimoto, J. G. Ultrahigh Resolution OCT Markers of Normal Aging and Early Age-Related Macular Degeneration. *Ophthalmol. Sci.* **2023**, *3* (3), 100277.
15. Miranda, M.; Santos-Oliveira, J.; Mendonça, A. M.; Sousa, V.; Melo, T.; Carneiro, Â. Human versus Artificial Intelligence: Validation of a Deep Learning Model for Retinal Layer and Fluid Segmentation in Optical Coherence Tomography Images from Patients with Age-Related Macular Degeneration. *Diagnostics* **2024**, *14* (10), 975.
16. Mukherjee, S.; De Silva, T.; Duic, C.; Jayakar, G.; Keenan, T. D. L.; Thavikulwat, A. T.; Chew, E.; Cukras, C. Validation of Deep Learning–Based Automatic Retinal Layer Segmentation Algorithms for Age-Related Macular Degeneration with 2 Spectral-Domain OCT Devices. *Ophthalmol. Sci.* **2024**, *5* (3), 100670.
17. De Silva, T.; Jayakar, G.; Grisso, P.; Hotaling, N.; Chew, E. Y.; Cukras, C. A. Deep Learning-Based Automatic Detection of Ellipsoid Zone Loss in Spectral-Domain OCT for Hydroxychloroquine Retinal Toxicity Screening. *Ophthalmol. Sci.* **2021**, *1* (4),
18. Ehlers, J. P.; Hu, A.; Boyer, D.; Cousins, S. W.; Waheed, N. K.; Rosenfeld, P. J.; Brown, D.; Kaiser, P. K.; Abbruscato, A.; Gao, G.; Heier, J.; ReCLAIM-2 (SPIAM-202) Study Investigators. ReCLAIM-2: A Randomized Phase II Clinical Trial Evaluating Elamipretide in Age-Related Macular Degeneration, Geographic Atrophy Growth, Visual Function, and Ellipsoid Zone Preservation. *Ophthalmol. Sci.* **2025**, *5* (1), 100628.
19. Fu, D. J.; Glinton, S.; Lipkova, V.; Faes, L.; Liefers, B.; Zhang, G.; Pontikos, N.; McKeown, A.; Scheibler, L.; Patel, P. J.; Keane, P. A.; Balaskas, K. Deep-Learning Automated Quantification of Longitudinal OCT Scans Demonstrates Reduced RPE Loss Rate, Preservation of Intact Macular Area and Predictive Value of Isolated Photoreceptor Degeneration in Geographic Atrophy Patients Receiving C3 Inhibition Treatment. *Br. J. Ophthalmol.* **2024**, *108* (4), 536–545.
20. Orlando, J. I.; Gerendas, B. S.; Riedl, S.; Grechenig, C.; Breger, A.; Ehler, M.; Waldstein, S. M.; Bogunović, H.; Schmidt-Erfurth, U. Automated Quantification of Photoreceptor Alteration in Macular Disease Using Optical Coherence Tomography and Deep Learning. *Sci. Rep.* **2020**, *10* (1), 5619.
21. Wang, Z.; Camino, A.; Zhang, M.; Wang, J.; Hwang, T. S.; Wilson, D. J.; Huang, D.; Li, D.; Jia, Y. Automated Detection of Photoreceptor Disruption in Mild Diabetic Retinopathy on Volumetric Optical Coherence Tomography. *Biomed. Opt. Express* **2017**, *8* (12), 5384–5398.
22. Zhang, G.; Fu, D. J.; Liefers, B.; Faes, L.; Glinton, S.; Wagner, S.; Struyven, R.; Pontikos, N.; Keane, P. A.; Balaskas, K. Clinically Relevant Deep Learning for Detection and Quantification of Geographic Atrophy from Optical Coherence Tomography: A Model Development and External Validation Study. *Lancet Digit. Health* **2021**, *3* (10), e665–e675.
23. Kalra, G.; Cetin, H.; Whitney, J.; Yordi, S.; Cakir, Y.; McConville, C.; Whitmore, V.; Bonnay, M.; Reese, J. L.; Srivastava, S. K.; Ehlers, J. P. Automated Identification and Segmentation of Ellipsoid Zone At-Risk Using Deep Learning on SD-OCT for Predicting Progression in Dry AMD. *Diagn. Basel Switz.* **2023**, *13* (6), 1178.

Disclaimer/Publisher's Note: The statements, opinions and data contained in all publications are solely those of the individual author(s) and contributor(s) and not of MDPI and/or the editor(s). MDPI and/or the editor(s) disclaim responsibility for any injury to people or property resulting from any ideas, methods, instructions or products referred to in the content.

© 2026 by the author(s). Distributed under a Creative Commons CC BY license.